The Effect of Turbulence on the Collision Rates of Small Cloud Drops

A. S. KOZIOL

Atmospheric Environment Service, Dorval, Quebec, Canada

H. G. LEIGHTON

Department of Atmospheric and Oceanic Sciences, McGill University, Montreal, Quebec, Canada

(Manuscript received 27 March 1995, in final form 18 January 1996)

ABSTRACT

The significance of the influence of turbulence on collisions and coalescence of small cloud droplets is still an outstanding problem. In particular, the growth of droplets in the radius range from 10 to 15 μm is not well understood. The present research examines whether or not turbulence affects the growth rate of such small drops by simulating trajectories of two hydrodynamically interacting droplets in a turbulent field. The trajectories were calculated with a model based on linear Stokes hydrodynamics. Turbulence was modeled in the form of random Fourier modes with both the space and time spectra prescribed. Both spectra were characterized by Kolmogorov scaling. The space spectrum was modeled in the inertial and dissipation subranges. On the basis of scale analysis, only small-scale time variations were allowed, and the so-called Eulerian–Lagrangian time spectrum was applied. The results show that most collision rates increase moderately in a turbulent flow characterized by rates of energy dissipation of the order of 1, 10, and 100 cm^2 s^{-3}.

1. Introduction

For over 50 years, the influence of turbulence on the process of collision–coalescence of cloud drops has been discussed in the cloud physics community. Over these years no agreement has been reached on whether or not turbulence is a major factor in the process of collisional growth of cloud droplets. Here we consider the effects of turbulence that are limited to small scales only (of the order of the Kolmogorov length scale). Turbulence on such scales is homogeneous, isotropic, and stationary. We do not consider, for example, the large-scale turbulent mixing of cloudy and cloud-free air. We also restrict the drop sizes of the collector (i.e., large) drops to the range 10–20 μm.

Historically, the first attempts to account for the influence of small-scale turbulence on the collisional growth of cloud drops were concentrated on the effect of drop inertia, by Arenberg (1939), Gabilly (1949), and the most comprehensively by East and Marshall (1954). Later, however, Saffman and Turner (1956) noticed that this effect (i.e., different drop motions relative to the air) is only one possible effect of turbulence, the other being due to different drop motions with the air. While the former effect is determined by the rms turbulent velocity, the later is governed by the rate of energy dissipation. According to Saffman and Turner (1956), the effect of the motion relative to the air is small except for drops of significantly different sizes, and the effect of the motion with the air might be significant only for strong turbulence (e.g., for the rate of energy dissipation, ϵ, of the order of 1000 cm^2 s^{-3}). Neither Saffman and Turner (1956) nor the earlier researchers included the effect of hydrodynamic interactions in their estimates. It was not until 1975 that the effect of hydrodynamic interactions was incorporated. De Almeida (1976, 1979) developed a method of calculating collision rates on the basis of modeling individual trajectories. He found that the effect of weak turbulent fields (ϵ = 1 and 10 cm^2 s^{-3}) on collision rates was very strong and affected profoundly the development of cloud spectra. However, subsequent work (Pruppacher and Klett 1980; Lomaya et al. 1990) questioned some of de Almeida's assumptions, and the results were never fully accepted. More recently, the diffusion equation for a stochastic process was applied to the problem under consideration by Reuter et al. (1988). The work demonstrated a very weak effect of turbulence on collision rates. However, because the results were obtained for larger collector drops than those under consideration here (80–500 μm) and, also, because no hydrodynamic interactions were included, the results are of a limited relevance to the present work.

This research is inspired by the work of Saffman and Turner (1956) and of de Almeida (1976, 1979). In

Corresponding author address: Dr. H. G. Leighton, Department of Atmospheric and Oceanic Sciences, McGill University, 805 Sherbrooke Street West, Montreal, PQ H3A 2K6, Canada.
Email: henry@zephyr.meteo.mcgill.ca

particular, the flux method presented in the next section is based on the work by Saffman and Turner (1956), and in the use of individual drop trajectories to calculate collision rates we follow de Almeida (1976, 1979).

2. The model

a. The flux method

Following the ideas of Smoluchowski (1916) for Brownian coagulation, and those of Saffman and Turner (1956), one can calculate the collision rate of drops 1 and 2 as a flux of droplets 2 through the sphere of radius $R = r_1 + r_2$ times the concentration of drops 1, n_1. (Here r_1 and r_2 are the radii of the collector and collected drops, respectively, and θ is the azimuthal angle for spherical coordinates.) This is of course true if there are no hydrodynamic interactions—otherwise the concentration of drops 2 in the vicinity of a collector drop 1 is not equal to the ambient concentration n_2. Therefore, we increase the radius R to allow for hydrodynamic interactions. Term R now represents a minimum radius beyond which the effect of hydrodynamic interactions between drops on their relative displacement can be neglected in comparison to the effects of turbulence. We are interested in the flux of drops 2 entering the sphere of radius R that subsequently collide with drops 1 at the origin. The flux through a surface element of the sphere, $d\mathbf{S}$, is represented by

$$d\mathcal{P} = -\mathbf{j}\cdot d\mathbf{S}\delta t P(\mathbf{S}), \tag{1}$$

where $\mathbf{j}$ is the average current of droplets 2 and $P(\mathbf{S})$ is the probability that drop 2 will collide with drop 1. Because $\mathbf{j} = n_2\mathbf{w}$, $\mathbf{w}$ being the average relative velocity of drops 1 and 2,

$$\mathcal{P} = -n_2\delta t \int_s P(\mathbf{S})\mathbf{w}\cdot d\mathbf{S}. \tag{2}$$

Provided that the separation between drops is not too large, and for the strengths of turbulence considered here, the average relative velocity of the drops is dominated by their terminal velocities and so

$$\mathbf{w}\cdot d\mathbf{S} = -(v_1 - v_2)dS\cos\theta \tag{3}$$

for all values of θ with significant probability of collision. (Here v_1 and v_2 are the respective terminal velocities of the drops, and θ is the azimuthal angle for spherical coordinates.) The largest values of θ occur for large radius ratios ($r_2/r_1 > 0.9$) and strong turbulence ($\epsilon = 100$ cm^2 s^{-3}), but even then $\theta < 40°$. Making the approximation in (2), we get

$$\mathcal{P} = 2\pi n_2\delta t R^2(v_1 - v_2)\int_0^\pi P(\theta; R)\cos\theta\sin\theta d\theta, \tag{4}$$

where, because of symmetry, $P(\mathbf{S}) = P(\theta; R)$.

We can interpret $\mathcal{P}$ as the probability that a droplet 2 collides with a droplet 1 during the time δt. This interpretation allows us to relate $\mathcal{P}$ to the collision kernel in the stochastic growth equation (Gillespie 1975)

$$K_{12}n_2\delta t = \mathcal{P}, \tag{5}$$

where K_{12} is the collision kernel. Finally,

$$K_{12} = \pi R^2(v_1 - v_2)\int_0^\pi P(\theta; R)\sin 2\theta d\theta. \tag{6}$$

By analogy to the case of laminar settling in a still fluid, we can define the collision efficiency for the turbulent case

$$E_{12} = \frac{K_{12}}{\pi(r_1 + r_2)^2(v_1 - v_2)} = \frac{R^2}{(r_1 + r_2)^2}\int_0^\pi P(\theta; R)\sin 2\theta d\theta. \tag{7}$$

As discussed in section 3, generally R is taken to be $20r_1$. To confirm that the results are not sensitive to the choice of R, we verified that calculations with $R = 10r_1$ gave collision efficiencies that agreed within statistical uncertainties with those obtained for $R = 20r_1$.

From (7), it is clear that $P(\theta; R)$ is the quantity that needs to be estimated with our hydrodynamic model. With the help of this model we will be able to perform trajectory calculations with the collector drop placed initially at the origin and the collected drop on the surface of the sphere of radius R at a specified angle θ. From many independent trajectory calculations, the probability is estimated as

$$P(\theta; R) = \frac{N_{\text{coll}}}{N_{\text{exp}}}, \tag{8}$$

where N_{coll} is the number of trajectories that resulted in collisions and N_{exp} is the total number of experiments–trajectories.

b. Scale analysis

For the sizes of drops considered here, the Reynolds numbers defined by the drop radii and terminal velocities are smaller than 0.06. Therefore, the use of Stokesian hydrodynamics is justified. Also, let us introduce scales characterizing both binary collision between drops and turbulence. According to convention (Jonas and Goldsmith 1972), the length and time scales for a two-drop problem are defined by

$$\mathcal{L} = \frac{(10r_1)v_1}{v_1 - v_2} \quad \mathcal{T} = \frac{10r_1}{v_1 - v_2}. \tag{9}$$

Note that the difference in terminal velocities represents the velocity scale. The characteristic scales of turbulence are defined, respectively, by the Kolmogorov length, time, and velocity as follows:

$$\eta_K = \left(\frac{\nu^3}{\epsilon}\right)^{1/4} \quad \tau_K = \left(\frac{\nu}{\epsilon}\right)^{1/2} \quad v_K = (\nu\epsilon)^{1/4}, \quad (10)$$

where ϵ is the rate of energy dissipation and ν is the kinematic viscosity. In Figs. 1–3, the three scales for the two-drop problem are juxtaposed with the Kolmogorov scales for different strengths of turbulence. The length scales for the two-drop interaction are similar to the turbulence length scales. In terms of turbulence spectra this means that the region to be modeled is the dissipation subrange and the upper range of the inertial subrange. We can also see that for the problem at hand the time variation of the turbulent field is much less important than its space variation.

c. *The resistance problem for two drops*

Because both the Reynolds number and the Strouhal number are small, the time-independent Stokes equation can be used to calculate forces and torques at each time instant. The linear character of the Stokes equation has beneficial consequences for the process of obtaining hydrodynamic forces, couples, and consequently drop trajectories. Let us expand the ambient turbulent flow in a Taylor series. (Scale analysis showed that the turbulent eddies of interest here are of the order of, or smaller than, the Kolmogorov length scale, and, therefore, the turbulent velocity field changes on such scales in a linear manner.) The two first terms of the series are

$$u_i(\mathbf{x}) = u_i(\mathbf{x}_0) + \frac{\partial u_i}{\partial x_j}\,\delta x_j + o(\delta^2 x). \quad (11)$$

Upon defining the rate of stress tensor and the solid-body angular velocity as

$$\mathbf{E}_\infty = E_{ij}^\infty = \frac{1}{2}\left(\frac{\partial u_i}{\partial x_j} + \frac{\partial u_j}{\partial x_i}\right)$$

and

$$\mathbf{\Omega}_\infty = \Omega_k^\infty = \frac{1}{2}\left(\frac{\partial u_i}{\partial x_j} - \frac{\partial u_j}{\partial x_i}\right), \quad (12)$$

respectively, (11) results in

$$u_i = u_i(x_0) + \mathbf{E}_\infty \cdot \delta\mathbf{x} + \mathbf{\Omega}_\infty \times \delta\mathbf{x}. \quad (13)$$

After Kim and Karrila (1991), the forces, couples, and stresslets for a flow in the form of (13) can be represented by the following matrix equation:

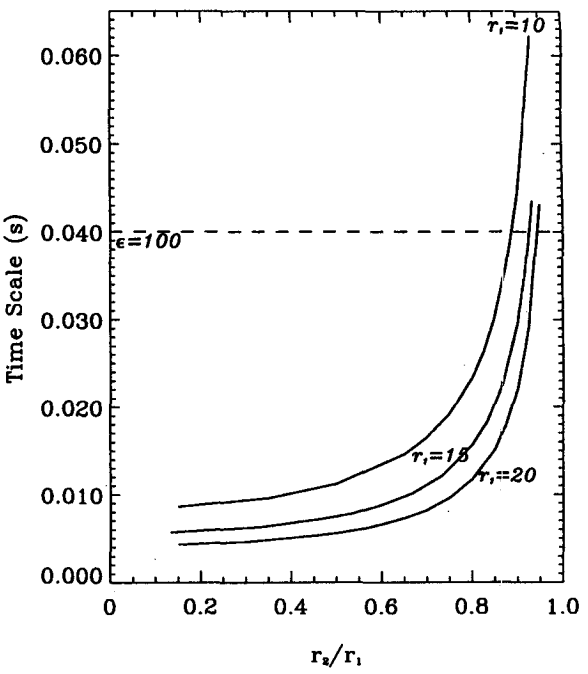

FIG. 2. Comparison of the two-drop timescales for different drops (solid lines) with the Kolmogorov timescales for different strengths of turbulence (dashed line; values for ϵ = 1 and 10 cm^2 s^{-3} are off-scale).

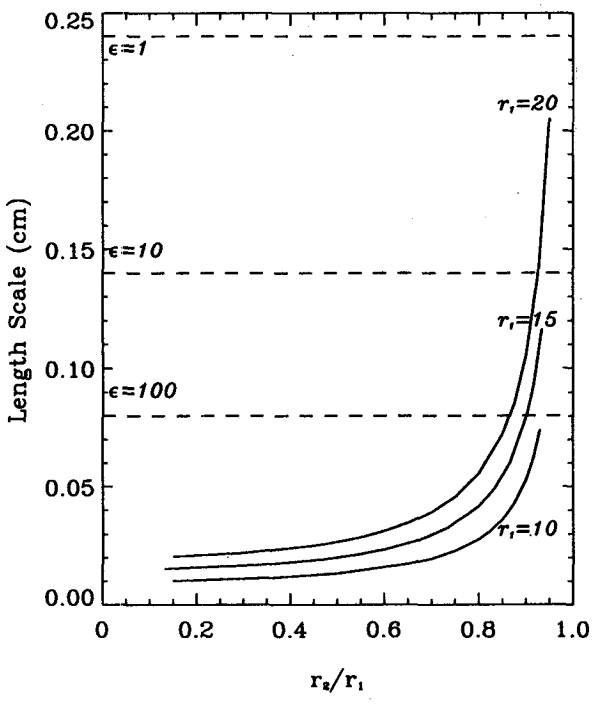

FIG. 1. Comparison of the two-drop length scales for different drops (solid lines) with the Kolmogorov length scales for different strengths of turbulence (dashed lines).

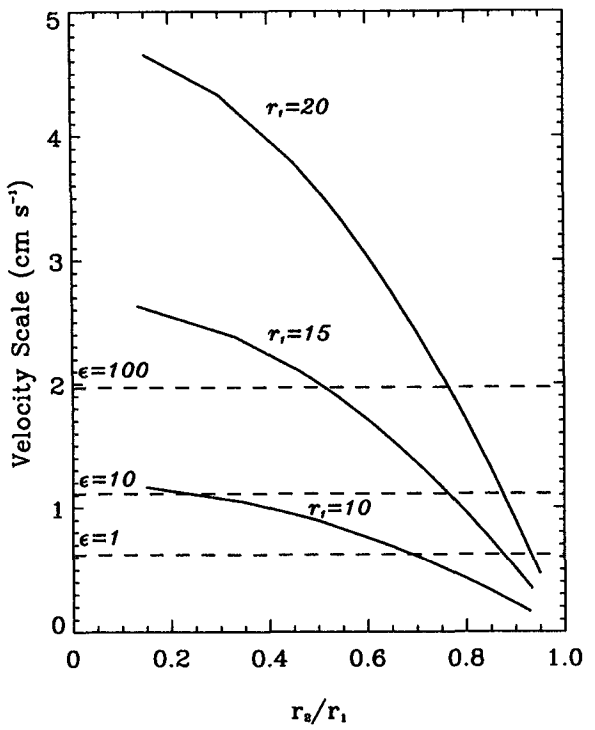

FIG. 3. Comparison of the terminal velocity differences for different pairs of drops (solid lines) with the Kolmogorov velocity scales for different strengths of turbulence (dashed lines).

$$\begin{pmatrix} \mathbf{F}_1 \\ \mathbf{F}_2 \\ \mathbf{T}_1 \\ \mathbf{T}_2 \\ \mathbf{S}_1 \\ \mathbf{S}_2 \end{pmatrix} = -\mu \begin{pmatrix} \mathbf{A}_{11} & \mathbf{A}_{12} & \tilde{\mathbf{B}}_{11} & \tilde{\mathbf{B}}_{12} & \tilde{\mathbf{G}}_{11} & \tilde{\mathbf{G}}12 \\ \mathbf{A}_{21} & \mathbf{A}_{22} & \tilde{\mathbf{B}}_{21} & \tilde{\mathbf{B}}_{22} & \tilde{\mathbf{G}}_{21} & \tilde{\mathbf{G}}22 \\ \mathbf{B}_{11} & \mathbf{B}_{12} & \mathbf{C}_{11} & \mathbf{C}_{12} & \tilde{\mathbf{H}}_{11} & \tilde{\mathbf{H}}_{12} \\ \mathbf{B}_{21} & \mathbf{B}_{22} & \mathbf{C}_{21} & \mathbf{C}_{22} & \tilde{\mathbf{H}}_{21} & \tilde{\mathbf{H}}_{22} \\ \mathbf{G}_{11} & \mathbf{G}_{12} & \mathbf{H}_{11} & \mathbf{H}_{12} & \mathbf{M}_{11} & \mathbf{M}_{12} \\ \mathbf{G}_{21} & \mathbf{G}_{22} & \mathbf{H}_{21} & \mathbf{H}_{22} & \mathbf{M}_{21} & \mathbf{M}_{22} \end{pmatrix} \times \begin{pmatrix} v_1 - \mathbf{u}(\mathbf{x}_1) \\ v_2 - \mathbf{u}(\mathbf{x}_2) \\ \Omega_1 - \Omega_\infty \\ \Omega_2 - \Omega_\infty \\ -\mathbf{E}_\infty \\ -\mathbf{E}_\infty \end{pmatrix}, \quad (14)$$

where μ is the dynamic viscosity, $\mathbf{A}$, $\mathbf{B}$, and $\mathbf{C}$ are second-rank tensors, $\mathbf{G}$ and $\mathbf{H}$ are third-rank tensors, and $\mathbf{M}$ is a fourth-rank tensor. (Stresslets are included only for the sake of completeness but have no bearing on the collision problem.) The positively defined matrix in (14) is called the grand matrix. One can prove that the following symmetry relations hold (Kim and Karrila 1991):

$$A_{ij}^{\alpha\beta} = A_{ji}^{\beta\alpha} \quad (15)$$

$$B_{ij}^{\alpha\beta} = \tilde{B}_{ji}^{\beta\alpha} \quad (16)$$

$$C_{ij}^{\alpha\beta} = C_{ji}^{\beta\alpha} \quad (17)$$

$$G_{ijk}^{\alpha\beta} = \tilde{G}_{kij}^{\beta\alpha} \quad (18)$$

$$H_{ijk}^{\alpha\beta} = H_{kij}^{\beta\alpha} \quad (19)$$

$$M_{ijkl}^{\alpha\beta} = M_{klij}^{\beta\alpha}. \quad (20)$$

Note that in the above equations superscripts α and β denote droplets and corresponds to subscripts 1 and 2 in (14).

The geometry of two drops possesses an intrinsic symmetry—the line through the centers being an axis of symmetry. Because of this the tensors contained in the grand matrix can be easily expressed with the help of scalar resistance functions (SRFs) as follows (Kim and Karrila 1991):

$$A_{ij}^{\alpha\beta} = X_{\alpha\beta}^{A} d_i d_j + Y_{\alpha\beta}^{A}(\delta_{ij} - d_i d_j) \quad (21)$$

$$B_{ij}^{\alpha\beta} = Y_{\alpha\beta}^{B} \epsilon_{ijk} d_k \quad (22)$$

$$C_{ij}^{\alpha\beta} = X_{\alpha\beta}^{C} d_i d_j + Y_{\alpha\beta}^{C}(\delta_{ij} - d_i d_j) \quad (23)$$

$$G_{ijk}^{\alpha\beta} = X_{\alpha\beta}^{G}\left(d_i d_j - \frac{1}{3}\delta_{ij}\right) + Y_{\alpha\beta}^{G}(d_i\delta_{jk} + d_j\delta_{ik} - 2d_i d_j d_k) \quad (24)$$

$$H_{ijk}^{\alpha\beta} = Y_{\alpha\beta}^{H}(\epsilon_{ikl} d_j + \epsilon_{jkl} d_i) d_l, \quad (25)$$

where vector d_i is the unit vector along the line of centers. [An analogous expression for M_{ijkl} can be found in Kim and Karrila (1991).] The SRFs $X_{\alpha\beta}$ and $Y_{\alpha\beta}$ have a straightforward association with simple types of motion such as motion along the line of centers, perpendicular to the line of centers, rotation, etc.

According to the above formulation of the resistance problem, and also including gravity g_i, we formally write the set of equations that completely describe the motion of two interacting droplets

$$m_\alpha \frac{dv_i^\alpha}{dt} = F_i^\alpha + m_\alpha g_i, \quad (26)$$

$$I_\alpha \frac{d\Omega_i^\alpha}{dt} = T_i^\alpha, \quad (27)$$

$$\frac{dx_i^\alpha}{dt} = v_i^\alpha, \quad (28)$$

where

$$F_i^\alpha = \mu A_{ij}^{\alpha\alpha}[u_j(\mathbf{x}^\alpha) - v_j^\alpha] + \mu A_{ij}^{\alpha\beta}[u_j(\mathbf{x}^\beta) - v_j^\beta] - \mu\tilde{B}_{ij}^{\alpha\alpha}(\Omega_j^\alpha - \Omega_j^\infty) - \mu\tilde{B}_{ij}^{\alpha\beta}(\Omega_j^\beta - \Omega_j^\infty) + \mu\tilde{G}_{ijk}^{\alpha\alpha} E_{jk}^\infty + \mu\tilde{G}_{ijk}^{\alpha\beta} E_{jk}^\infty, \quad (29)$$

$$T_i^\alpha = \mu B_{ij}^{\alpha\alpha}[u_j(\mathbf{x}^\alpha) - v_j^\alpha] + \mu B_{ij}^{\alpha\beta}[u_j(\mathbf{x}^\beta) - v_j^\beta] - \mu C_{ij}^{\alpha\alpha}(\Omega_j^\alpha - \Omega_j^\infty) - \mu C_{ij}^{\alpha\beta}(\Omega_j^\beta - \Omega_j^\infty) + \mu \tilde{H}_{ijk}^{\alpha\alpha} E_{jk}^\infty + \mu \tilde{H}_{ijk}^{\alpha\beta} E_{jk}^\infty. \quad (30)$$

The coefficients $A_{ij}^{\alpha\beta}$, $B_{ij}^{\alpha\beta}$, $\tilde{B}_{ij}^{\alpha\beta}$, $C_{ij}^{\alpha\beta}$, $\tilde{G}_{ij}^{\alpha\beta}$, and $\tilde{H}_{ij}^{\alpha\beta}$ can be expressed in terms of SRFs [(21)–(25)]. All the SRFs are calculated with no-slip boundary conditions. The functions $X_{\alpha\beta}^A$ were obtained by superposing the Stimson and Jeffery (1926) solution for spheres moving with equal velocities with the modified Maud (1961) solution for spheres moving with equal speeds in opposite directions. The functions $Y_{\alpha\beta}^A$ and $Y_{\alpha\beta}^B$ were obtained using the expressions of Davis (1969). The coefficients $X_{\alpha\beta}^C$ were calculated as in Jeffrey and Onishi (1984), and the coefficients $Y_{\alpha\beta}^G$, $Y_{\alpha\beta}^H$ as in Jeffrey (1992). All the SRFs depend only on two nondimensional parameters, the radius ratio, and the parameter, $2D/(r_1 + r_2)$, where D is the distance between centers.

d. Modeling of the turbulent velocity field

In this section, we present the method of random Fourier modes that is used to model the velocity field. Let the flow be represented by the series of random Fourier modes as follows (Kraichnan 1970):

$$u_i(\mathbf{x}, t) = \sum_{n=1}^{N} [b_i^{(n)} \cos(\mathbf{k}^{(n)}\cdot\mathbf{x} + \omega^{(n)}t) + c_i^{(n)} \sin(\mathbf{k}^{(n)}\cdot\mathbf{x} + \omega^{(n)}t)]. \quad (31)$$

After Maxey (1987), let the wavenumbers, k, and the frequencies, ω, be random variables with the probability density functions $p_1(\mathbf{k})$ and $p_2(\omega)$, respectively. The coefficients $b_i^{(n)}$ and $c_i^{(n)}$ must be chosen in such a way that the flow is incompressible, and the two-point velocity correlation corresponds to the desired energy spectrum. [Again we follow Maxey (1987).] The condition of incompressibility

$$\frac{\partial u_i}{\partial x_i} = 0 \Rightarrow \mathbf{b}^{(n)}\cdot\mathbf{k}^{(n)} = \mathbf{c}^{(n)}\cdot\mathbf{k}^{(n)} = 0 \quad (32)$$

is satisfied for coefficients of the form

$$b_i^{(n)} = \Gamma(k, \omega)\left(\delta_{ij} - \frac{k_i^{(n)} k_j^{(n)}}{k^{(n)2}}\right)\hat{b}_j^{(n)}. \quad (33)$$

The function $\Gamma(k, \omega)$ scales the coefficients so as to obtain the desired energy spectrum, while the coefficients $\hat{b}_j^{(n)}$ are random Gaussian variables with zero mean and unit variance (similar relations hold for $\hat{c}_j^{(n)}$). The derivation of $\Gamma(k, \omega)$ proceeds as follows. The four-dimensional (space–time) two-point correlation function for a velocity field is defined as

$$R_{ij}(\mathbf{r}, \tau) = \overline{u_i(\mathbf{x}, t)u_j(\mathbf{x} + \mathbf{r}, t + \tau)}, \quad (34)$$

where $u_i(\mathbf{x}, t)$ are the velocity components and the overbar represents the ensemble average. Let this velocity correlation tensor be written in the form

$$R_{ij}(\mathbf{r}, \tau) = \iiint_{-\infty}^{\infty} d^3\mathbf{k} \int_{-\infty}^{\infty} d\omega [p_1(\mathbf{k})p_2(\omega)u_i(\mathbf{x}, t) \times u_j(\mathbf{x} + \mathbf{r}, t + \tau)]. \quad (35)$$

Substituting (31) in (35) results in the following expression:

$$R_{ij}(r, \tau) = N \iiint_{-\infty}^{\infty} d^3\mathbf{k} \int_{-\infty}^{\infty} d\omega \left[p_1(\mathbf{k})p_2(\boldsymbol{\omega}) \times \Gamma^2(k, \omega)\left(\delta_{ij} - \frac{k_i k_j}{k^2}\right)\cos(\mathbf{k}\cdot\mathbf{r} + \omega\tau)\right]. \quad (36)$$

From the theory of homogeneous turbulence,

$$R_{ij}(\mathbf{r}, \tau) = \iiint_{-\infty}^{\infty} d^3\mathbf{k} \int_{-\infty}^{\infty} d\omega \Phi_{ij}(\mathbf{k}, \omega) e^{i(\mathbf{k}\cdot\mathbf{r} + \omega\tau)}, \quad (37)$$

where $\Phi_{ij}(\mathbf{k}, \omega)$ is the space–time spectrum. Further, on the basis of

$$\Phi_{ij}(\mathbf{k}, \omega) = \frac{\mathcal{E}(k, \omega)}{4\pi k^2}\left(\delta_{ij} - \frac{k_i k_j}{k^2}\right) \quad (38)$$

(Batchelor 1953), where $\mathcal{E}(k, \omega)$ is the four-dimensional kinetic energy spectrum, (37) can be rewritten as

$$R_{ij}(\mathbf{r}, \tau) = \iiint_{-\infty}^{\infty} d^3\mathbf{k} \int_{-\infty}^{\infty} d\omega \left[\frac{1}{4\pi k^2}\mathcal{E}(\mathbf{k}, \omega) \times \left(\delta_{ij} - \frac{k_i k_j}{k^2}\right)\cos(\mathbf{k}\cdot\mathbf{r} + \omega\tau)\right]. \quad (39)$$

Finally, a comparison of (36) and (39) gives the scaling function $\Gamma(k, \omega)$

$$\Gamma^2(k, \omega) = \frac{\mathcal{E}(k, \omega)}{4\pi k^2 N p_1(\mathbf{k})p_2(\omega)}. \quad (40)$$

The determination of the four-dimensional spectrum $\mathcal{E}(k, \omega)$ has to be based on the knowledge of the wavenumber (energy) spectrum, $E(k)$, and the frequency (time) spectrum, $\chi_{ii}(\omega)$. Note that

$$E(k) = \int_{-\infty}^{\infty} \mathcal{E}(k, \omega) d\omega$$

and

$$\chi_{ii}(\omega) = \iiint_{-\infty}^{\infty} \Phi_{ii}(\mathbf{k}, \omega) d^3\mathbf{k}. \quad (41)$$

We assume that the energy spectrum has the form of the Pao spectrum (Pao 1965)

$$E(k) = \alpha\epsilon^{2/3}k^{-5/3}\exp\left(-\frac{3}{2}\alpha\nu\epsilon^{-1/3}k^{4/3}\right). \quad (42)$$

This form was verified experimentally (Pao 1965) and has a convenient mathematical form. Measurements show that α is approximately equal to 1.5 (Grant et al. 1962; Gibson 1963). The spectrum given by (42) reduces to the $-5/3$ law for small wavenumbers.

The choice of form of the time spectrum is more complicated. It is believed that the Eulerian time spectrum behaves like ω^{-2}, while the Lagrangian time spectrum goes as $\omega^{-5/3}$ (Tennekes 1975; Nelkin 1992). The form of the Eulerian spectrum, according to Tennekes (1975) is due to the sweeping effect of large eddies (of the order of the integral scale of turbulence). Fortunately for us, because of the small scales that are considered here (of the order of the Kolmogorov scale), there is no need to worry about the sweeping effect of large scales. Therefore, even if the required time spectrum is Eulerian in nature, a mathematical expression similar to the Lagrangian spectrum will be applied. In this we follow Fung et al. (1992), who used for such a spectrum the term Eulerian–Lagrangian spectrum. The Eulerian–Lagrangian time spectrum then takes the form

$$\chi_{ii}^{\mathrm{EL}}(\omega) = \beta_{\mathrm{EL}}\epsilon\omega^{-2}. \quad (43)$$

Implicitly it is assumed that the small scales under consideration and the eddy-containing large scales are decorrelated for the purpose of our investigation. The frequency spectrum has a cutoff equal to the inverse of the Kolmogorov timescale (Tennekes and Lumley 1972).

In order to obtain an expression for $\mathcal{E}(k, \omega)$, that combines both spectra we follow the method by Fung et al. (1992). They assume that frequency is spread in a Gaussian manner with variance σ_ω^2 around the characteristic frequency $\bar{\omega}$. (Both parameters of the distribution are functions of k.) The spectrum $\mathcal{E}(k, \omega)$ is then

$$\mathcal{E}(k, \omega) = E(k)\frac{1}{(2\pi)^{1/2}\sigma_\omega} \times \exp\left[-\frac{(\omega - \bar{\omega})^2}{2\sigma_\omega^2}\right]. \quad (44)$$

Fung et al. (1992) assume after Leslie (1973) that

$$\sigma_\omega = \bar{\omega} = \epsilon^{1/3}k^{2/3}. \quad (45)$$

The numerical calculation of Fung et al. shows that the above choice of $\mathcal{E}(k, \omega)$ results in the Eulerian–Lagrangian spectrum (43).

Equation (40) will now be complete if the wavenumber and frequency probability density functions are specified. In comparison with Maxey (1987), where a very narrow Gaussian-type wavenumber spectrum was used, and $p_1(k)$ and $p_2(\omega)$ were also Gaussian, the problem at hand requires relatively wide spectral bands. This suggests that all three wavenumber components and the frequency be distributed with rectangular distributions in their respective ranges: ($k_l \leq k_i \leq k_0$; $-k_0 \leq k_i \leq -k_l$) and ($\omega_l \leq \omega \leq \omega_0$; $-\omega_0 \leq \omega \leq -\omega_l$). While the magnitude of ω_0 is determined by the viscous cutoff (the inverse of the Kolmogorov timescale), the determination of the magnitude of k_0 calls for a more laborious approach. With higher and higher wavenumbers, the amplitude of the motion as well as of the velocity gradient become smaller and smaller. Criteria based on both amplitude and velocity gradient are used to perform the truncation of high wavenumbers. Lower limits of the wavenumber components and frequency are determined by the inverse of the scale characterizing energy-containing eddies. Crude estimates of the above are

$$k_l = \frac{1}{l_l} = \frac{\epsilon}{q^3}$$

and

$$\omega_l = \frac{1}{t_l} = \frac{q}{l} = \frac{\epsilon}{q^2}, \quad (46)$$

where q is the rms velocity that for a developing cumulus cloud ranges between 1 and 10 m s^{-1}. The model is insensitive to the choice of k_l and ω_l, and thus, the choice of q is not very important. (Terms k_l and ω_l are at least 10^4 times smaller than k_0 and ω_0.)

Finally substituting (44), (42), and the probability density functions

$$p_1(k) = \frac{1}{(2k_0)^3}$$

and

$$p_2(\omega) = \frac{1}{2\omega_0} \quad (47)$$

in (40), the equation for the scaling function $\Gamma(k, \omega)$ is

$$\Gamma^2(k, \omega) = \frac{4}{(2\pi^3)^{1/2}}\frac{\alpha k_0^3\omega_0\epsilon^{2/3}}{N}\epsilon^{1/3}k^{-13/3} \times \exp\left(-\frac{3}{2}\alpha\nu\epsilon^{-1/3}k^{-4/3}\right) \times \exp\left[-\frac{(\omega - \epsilon^{-1/3}k^{2/3})^2}{2\epsilon^{2/3}k^{4/3}}\right]. \quad (48)$$

Note that in (47), it was assumed that k_l and ω_l are much smaller than k_0 and ω_0, and thus $k_l = \omega_l \approx 0$. The nondimensional lower and upper limits of the wavenumbers and frequency (scaled by the inverse of the Kolmogorov length and time, respectively) used in the calculation are $10^{-4} < k_i < 1.8$ and $10^{-6} < \omega < 1$. The number of Fourier modes, after considering both

the time of calculation and the representation of the turbulent field, was chosen to be 2000.

The average space and time spectra for 20 000 realizations of the turbulent field are presented in Fig. 4. The appropriate slopes (i.e., $-5/3$ for the wavenumber spectrum and -2 for the frequency spectrum) are included for comparison. The range of wavenumbers covers the dissipation subrange as well as the transition region between the inertial and dissipation subranges. The pure inertial range is not modeled. Therefore, the wavenumber spectrum is steeper than the $-5/3$ slope. The time spectrum captures relatively well the -2 slope. Also, for smaller frequencies, the tendency of the time spectrum to follow the less steep $-5/3$ slope is visible. This is due to the sweeping effect of larger eddies. When using the velocity field to model drop trajectories, truncations based on the scales of two-drop interactions were introduced (i.e., scales much larger than the respective length and timescales of drop interaction were truncated). In many circumstances, drops did not encounter a time variation, while in others, notably when the interacting drops had similar sizes, only the smallest timescales were included.

3. Calculations

In the previous section, we described the structural elements of the model. In particular, we introduced a statistical approach that allows us to calculate collision kernels for known values of the probability of collision as a function of the azimuthal angle, θ. The role of the dynamic model was to facilitate the calculation of this probability. This was accomplished through multiple repetitions of the same experiment for different realizations of the turbulent velocity field. In each experiment, the large drop was placed at the origin and the small drop at a point (R, θ, ϕ). The coordinate θ was varied, but ϕ was always assumed to be 0° because of symmetry in ϕ. Then the initial value problem for two drops, (26)–(28), was solved up to the time when either the droplets collided or the large drop passed the small one, and there was no chance for the occurrence of a collision. We assumed that a collision occurred when the nondimensional distance between drop surfaces $\delta = S/r_1$ is equal to 0.001. The governing equations were solved with the help of a predictor (Adams–Bashfort)–corrector (Adams–Moulton) scheme (Shampine and Gordon 1975). After a sufficient number of trajectories were computed, the probability of collision $P(\theta; R)$ was estimated. The subsequent integration of $P(\theta; R)$ according to (6) and (7) but with a constant limit of integration $\theta_{\max}$ allowed us to obtain the collision kernels and collision efficiencies. However, before the numerical values could be obtained, a number of choices had to be made. These are the choice of the radius R, the truncation of turbulence modes that do not influence the relative motion of drops, the number and spacing of angles θ_i for the integration, the value of $\theta_{\max}$, and the number of experiments for each θ_i.

The choice of R was determined by two factors, the strength of the hydrodynamic interactions and the requirement that there be a sufficient number of collisions. Unlike the case of a still fluid, the turbulent case is not sensitive to weak interactions between drops at large separations. These can be neglected, because at large separations the relative displacements of drops due to the hydrodynamic interactions are much smaller than those due to turbulence. In the majority of calculations $R = 20r_1$. Only in situations in which the relative displacement of drops due to turbulence is much larger than the drop radii, for example, for drop radius ratios of the order or greater than 0.9, and for the rate of energy dissipation 10 and 100 cm^2 s^{-3}, $R = 10r_1$.

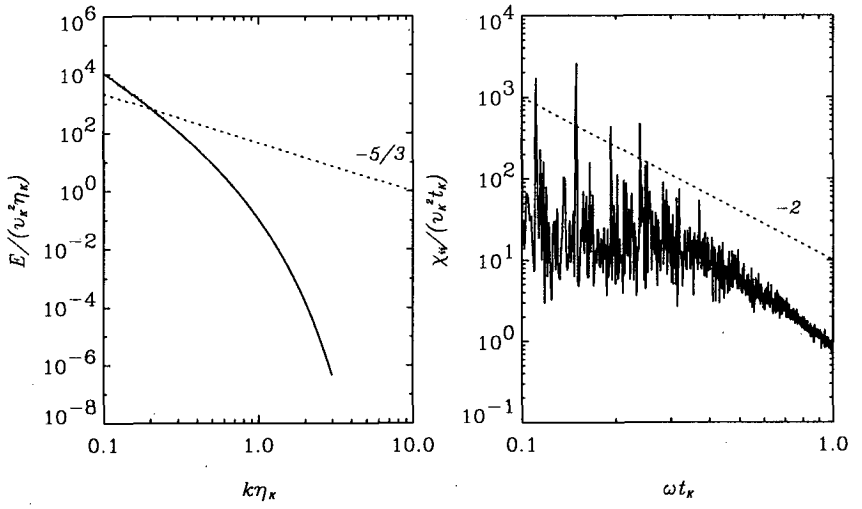

FIG. 4. The nondimensional wavenumber (E) and frequency (χ_{ii}) spectra.

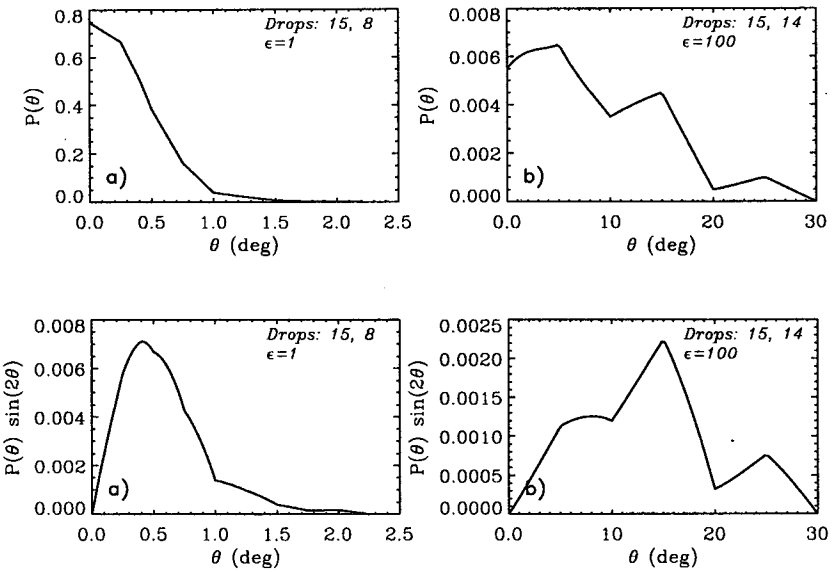

FIG. 5. Probability $P(\theta)$ and $P(\theta)$ sin2θ for a typical case of (a) weak turbulence ($r_1 = 15$ μm, $r_2 = 8$ μm, $\epsilon = 1$ cm^2 s^{-3}) and (b) strong turbulence ($r_1 = 15$ μm, $r_2 = 14$ μm, $\epsilon = 100$ cm^2 s^{-3}).

Truncation of the turbulence modes was dictated by the necessity to limit computer time. Different drop pairs are characterized by different time and length scales of interaction. Therefore, the range of the Fourier modes that actively participate in binary drop interactions vary. There is no need to include those modes that have timescales and length scales much larger than the scales of interaction because they do not contribute to the relative displacement but merely impose a background velocity field, identical for both drops. The practical criterion that we applied was that all the scales larger than 50 times the scales of interaction were truncated.

The specifications of the angles θ_i and θ_{max} and the number of experiments were based on subjective judgment. Initially, we started with θ_i uniformly distributed in what we anticipated to be the range of nonzero probability of collision. Then, looking at the curve $P(\theta)$ sin2θ versus θ, decisions concerning addition of extra points were made. This type of a subjective judgment worked well for the "weak turbulence" cases (smooth curves) as opposed to the "strong turbulence" cases (noisy curves). (The weak-turbulence cases are those for which the length scale of the two-drop problem is larger than the Kolmogorov length scale. The opposite scale relation defines the strong-turbulence cases.) In Fig. 5, there are presented curves of $P(\theta)$ and $P(\theta)$ sin2θ versus θ for both weak- and strong-turbulence cases. In the latter category, error analysis was used in order to decide whether more values of θ needed to be examined, but, again, the final decisions were made in a rather arbitrary way. Finally, the number of experiments for each θ was based, again, on error analysis.

4. Results

We systematically examined collector drops with three different radii: 10, 15, and 20 μm. For each col-

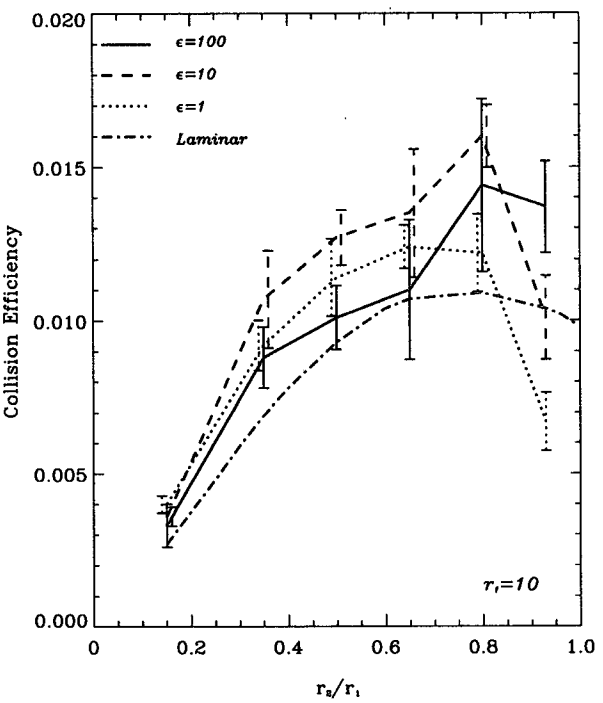

FIG. 6. Comparison of the collision efficiencies for different strengths of turbulence with the laminar collision efficiencies for 10-μm collector drops.

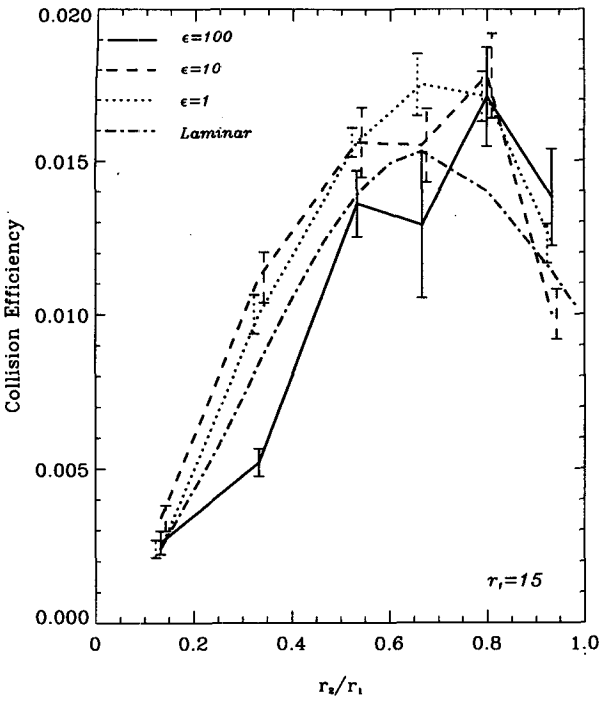

FIG. 7. Comparison of the collision efficiencies for different strengths of turbulence with the laminar collision efficiencies for 15-μm collector drops.

lector drop, there were chosen six to seven smaller drops for which we obtained the collision efficiencies. The selected rates of energy dissipation were 1, 10, and 100 cm^2 s^{-3}. Figures 6–8 compare the values of the collision efficiencies for the laminar and turbulent cases for the same collector drop. [Because of our representation of the hydrodynamic forces, our laminar calculations can be compared with the results of Hocking and Jonas (1970) for $\delta = 0.001$.]

For a 10-μm collector drop, a general increase in the collision efficiency is observed. The maximum increase is 50% for collisions with 8-μm drops, and $\epsilon = 10$ cm^2 s^{-3}. For $\epsilon = 1$ and 10 cm^2 s^{-3} and for large drop radius ratios, the collision efficiency decreases as r_2/r_1 increases, but for $\epsilon = 100$ cm^2 s^{-3} no such trend is evident. The shape of the collision efficiency curves for 15- and 20-μm collector drops is similar to that for 10-μm collector drops except that for large r_2/r_1 the collision efficiency decreases with increasing r_2/r_1 when $\epsilon = 100$ cm^2 s^{-3}. For a 15-μm collector drop the effect is generally weaker than for a 10-μm collector drop, especially for $\epsilon = 10$ and 100 cm^2 s^{-3}. The largest relative increase in collision efficiency (60%) is found for 20-μm collector drops collecting 16-μm drops with $\epsilon = 100$ cm^2 s^{-3}. The maximum in the collision efficiency curves for $\epsilon = 1$ cm^2 s^{-3} occurs at about the same value of r_2/r_1 as for the laminar collision efficiency for all three values of r_1. For stronger turbulence, the maxima in the collision efficiency curves are shifted to larger values of r_2/r_1 relative to the maxima for laminar flow.

For $\epsilon = 1$ cm^2 s^{-3}, the calculated statistical errors are of the order of a few percent. For the majority of cases with stronger turbulence ($\epsilon = 10$ and 100 cm^2 s^{-3}), the errors are between 10% and 15%. Only for collector drops of radii 10 μm and $\epsilon = 100$ cm^2 s^{-3} are the errors larger, between 15% and 20% for some radius ratios.

From the point of view of the stochastic growth equation, the collision kernels provide more physical insight than the collision efficiencies. This is because they are proportional to the collision rates. We provide the collision kernels (K_{12}) for all three strengths of turbulence (100, 10, and 1 cm^2 s^{-3}) and laminar flow in Fig. 9. The tendencies observed for the collision kernels are obviously the same as those for the collision efficiencies. We do, however, point out the general trend that makes the turbulent collision kernel curves more flat in the middle range of radius ratios in comparison to the laminar collision kernels curves as turbulence becomes more vigorous. In other words, for strong turbulence, the collision kernels tend to be independent of radius ratio in the range of radius ratios from 0.3 to 0.8.

5. Conclusions

Presently, the only systematic and comprehensive examination of the influence of turbulence on collision

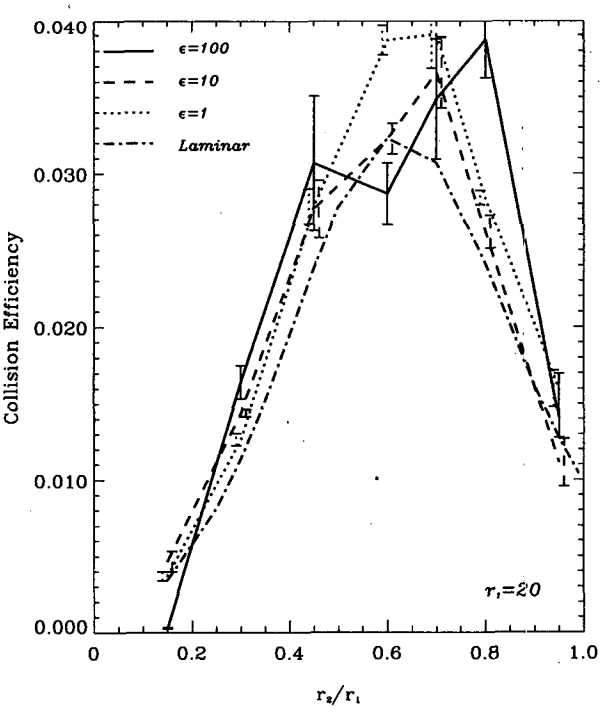

FIG. 8. Comparison of the collision efficiencies for different strengths of turbulence with the laminar collision efficiencies for 20-μm collector drops.

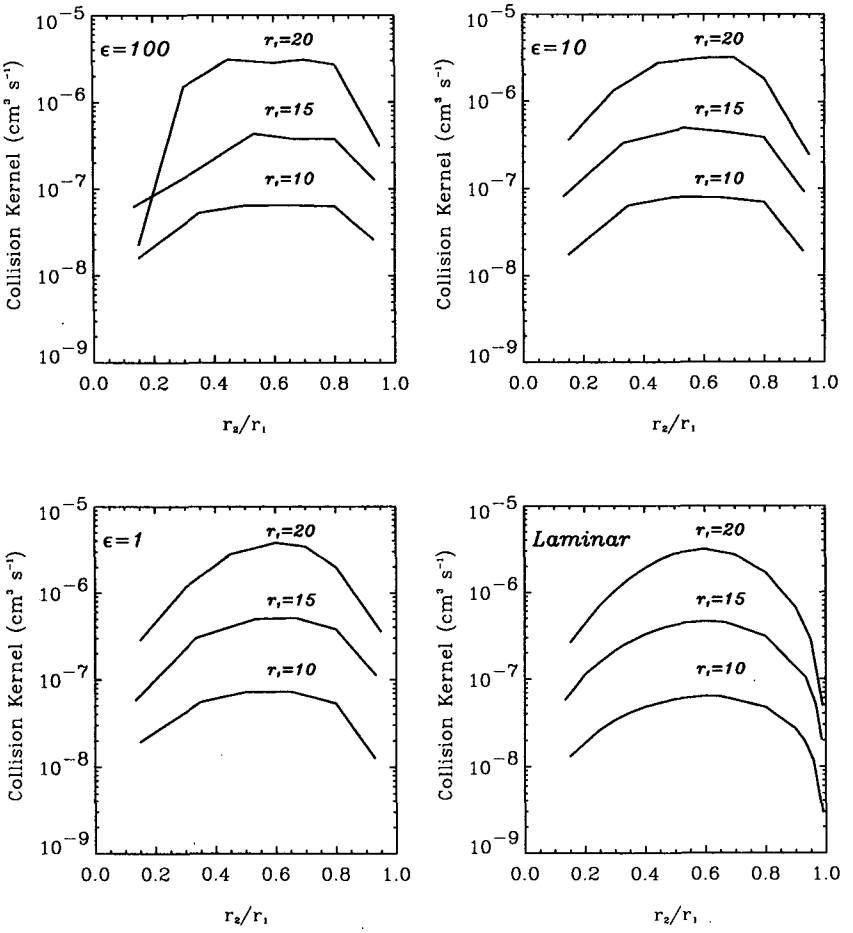

FIG. 9. Collision kernels for turbulent flows with different rates of energy dissipation (ϵ = 100, 10, 1 cm^2 s^{-3}) and for laminar flow.

efficiencies is that by de Almeida (1976, 1979). The effect of turbulence that de Almeida's drops experienced was dramatic—the increase of collision efficiencies being tenfold and larger. Such large increases were not found here. Our model predicts moderate, at maximum 1.5-fold increases, and, for some combinations of drop radii and rate of energy dissipation, our model even predicts decreases in the collision efficiency.

Let us summarize our results in a concise way. Weak turbulence (ϵ = 1 cm^2 s^{-3}), with a few exceptions, causes a moderate and relatively uniform increase of the collision efficiencies for all examined collector drops. For stronger turbulence, the behavior is more complex. For ϵ = 10 cm^2 s^{-3}, the largest relative increase is found for collector drops of 10-μm radii; while for ϵ = 100 cm^2 s^{-3}, for collector drops of 20-μm radii. The maxima of the collision efficiency are shifted toward larger radius ratios when compared to the laminar collision efficiency curves.

A detailed interpretation of the shapes of the collision efficiency curves is not justified because of the relatively large statistical uncertainties. Nevertheless, it is worth noting that part of the complexity of the curves may be due to the fact that within the present framework turbulence can influence the collision process either through its effect on gravitational settling or as a result of its direct effect on the hydrodynamic interactions. Each of these mechanisms may depend in a complicated way on the droplet radii and strength of the turbulence. To gain a more complete understanding of the shapes of the curves, many more lengthy and computationally expensive experiments would be required. In view of the relatively small influence that turbulence of the intensity considered here has on the collision rates of small drops, further experimentation is not warranted. Our interest is in the potential of turbulence to influence the development of drop size spectra. We do not expect a pronounced effect of these new collision efficiencies on the growth of droplet spectra because the values of the turbulent collision efficiencies differ relatively little from the values for laminar flow. The differences between the laminar and turbulent collision

efficiencies are, for example, smaller than those resulting from the introduction of gas kinetic effects by Davis (1972), which were subsequently shown to have only a small impact on cloud droplet spectrum evolution (Leighton 1977).

Acknowledgments. The authors gratefully acknowledge Prof. D. J. Jeffrey of the Department of Applied Mathematics at the University of Western Ontario, Canada, for the help in the area of the low Reynolds number flows as well as for the FORTRAN code to calculate the scalar resistance functions. This work was supported by a grant from the Natural Sciences and Engineering Research Council. Computer time on the NEC-SX3 supercomputer was provided by the Canadian Atmospheric Environment Service.

REFERENCES

Arenberg, D., 1939: Turbulence as a major factor in the growth of cloud droplets. *Bull. Amer. Meteor. Soc.,* **20,** 444–445.

Batchelor, G. K., 1953: *The Theory of Homogeneous Turbulence.* Cambridge University Press, 197 pp.

Davis, M. H., 1969: The slow translation and rotation of two unequal spheres in a viscous fluid. *Chem. Eng. Sci.,* **24,** 1769–1776.

——, 1972: Collisions of small cloud droplets: Gas kinetic effects. *J. Atmos. Sci.,* **29,** 911–915.

de Almeida, F. C., 1976: The collision problem in cloud droplets moving in a turbulent environment. Part I: A method of solution. *J. Atmos. Sci.,* **33,** 1571–1878.

——, 1979: The collisional problem of cloud droplets moving in a turbulent environment. Part II: Turbulent collision efficiencies. *J. Atmos. Sci.,* **36,** 1564–1576.

East, T. W. R., and J. S. Marshall, 1954: Turbulence in clouds as a factor in precipitation. *Quart. J. Roy. Meteor. Soc.,* **80,** 26–47.

Fung, J. C. H., J. C. R. Hunt, N. A. Malik, and R. J. Perkins, 1992: Kinematic simulation of homogeneous turbulence by unsteady random Fourier modes. *J. Fluid Mech.,* **236,** 281–318.

Gabilly, A., 1949: On the role that turbulence can play in the coalescence of cloud droplets. *Ann. Geophys.,* **5,** 232–234.

Gibson, M. M., 1963: Spectra of turbulence in a round jet. *J. Fluid Mech.,* **15,** 161–173.

Gillespie, D. T., 1975: Three models of the coalescence growth of cloud droplets. *J. Atmos. Sci.,* **32,** 600–607.

Grant, H. L., R. W. Stewart, and A. Moilliett, 1962: Turbulence spectra from a tidal channel. *J. Fluid Mech.,* **12,** 241–263.

Hocking, L. M., and P. R. Jonas, 1970: The collision efficiency of small drops. *Quart. J. Roy. Meteor. Soc.,* **96,** 722–729.

Jeffrey, D. J., 1992: The calculation of the low Reynolds number resistance functions for two unequal spheres. *Phys. Fluids A,* **4,** 16–29.

——, and Y. Onishi, 1984: Calculation of the resistance and mobility functions for two unequal rigid spheres in low Reynolds number flow. *J. Fluid Mech.,* **130,** 261–290.

Jonas, P. R., and P. Goldsmith, 1972: The collection efficiencies of small droplets falling through a sheared air flow. *J. Fluid Mech.,* **52,** 593–608.

Kim, S., and S. J. Karrila, 1991: *Microhydrodynamics: Principles and Selected Applications.* Butterworth-Heinemann, 507 pp.

Kraichnan, R. H., 1970: Diffusion by random velocity field. *Phys. Fluids,* **13,** 22–31.

Leighton, H. G., 1977: Collision efficiency and cloud spectrum evolution. *J. Atmos. Sci.,* **34,** 2005–2006.

Leslie, D. C., 1973: *Developments in the Theory of Turbulence.* Claredon Press, 367 pp.

Lomaya, V. A., I. P. Mazin, and A. I. Neizvestnyy, 1990: Effect of turbulence on the coagulation efficiency of cloud droplets. *Izv. Atmos. Oceanic Phys.,* **26,** 595–600.

Maud, A. D., 1961: End effects in falling-sphere viscometer. *Br. J. Appl. Phys.,* **12,** 293–295.

Maxey, M. B., 1987: The gravitational settling of aerosol particles in homogeneous turbulence and random flow fields. *J. Fluid Mech.,* **174,** 441–465.

Nelkin, M., 1992: In what sense is turbulence an unsolved problem? *Science,* **255,** 566–570.

Pao, Y.-H., 1965: Structure of turbulent velocity and scalar fields at large wavenumbers. *Phys. Fluids,* **8,** 1063–1075.

Pruppacher, H. R., and J. D. Klett, 1980: *Microphysics of Clouds and Precipitation.* Reidel, 714 pp.

Reuter, G. W., R. de Villiers, and Y. Yavin, 1988: The collection kernel for two falling cloud drops subjected to random perturbations in a turbulent air flow: A stochastic model. *J. Atmos. Sci.,* **45,** 765–773.

Saffman, P. G., and J. S. Turner, 1956: On the collision of drops in turbulent clouds. *J. Fluid Mech.,* **1,** 16–30.

Shampine, L. F., and M. K. Gordon, 1975: *Computer Solution of Ordinary Differential Equations. The Initial Value Problem.* W. H. Freeman, 444 pp.

Smoluchowski, M., 1916: Drei Vorträge über Diffusion Brownsche Molecularbewegung und Koagulation von Kolloidteilchen. *Phys. Z.,* **17,** 557–571.

Stimson, M., and G. B. Jeffery, 1926: The motion of two spheres in viscous fluid. *Proc. Roy. Soc. London,* **A111,** 110–116.

Tennekes, H., 1975: Eulerian and Lagrangian time microscales in isotropic turbulence. *J. Fluid Mech.,* **67,** 561–567.

——, and J. L. Lumley, 1972: *A First Course in Turbulence.* The MIT Press, 300 pp.